Modelling J/ψ production and absorption in a microscopic nonequilibrium approach

C. Spieles[1*†], R. Vogt[1,2], L. Gerland[3], S.A. Bass[4*], M. Bleicher[3], H. Stöcker[3], W. Greiner[3]

[1] *Nuclear Science Division, Lawrence Berkeley National Laboratory, Berkeley, CA 94720, USA*

[2] *Physics Department, University of California at Davis, Davis, CA 95616, USA*

[3] *Institut für Theoretische Physik, J. W. Goethe-Universität, D-60054 Frankfurt a.M., Germany*

[4] *Department of Physics, Duke University, Durham, N.C. 27708-0305, USA*

(October 17, 2005)

Abstract

Charmonium production and absorption in heavy ion collisions is studied with the Ultrarelativisitic Quantum Molecular Dynamics model. We compare the scenario of universal and time independent color-octet dissociation cross sections with one of distinct color-singlet J/ψ, ψ' and χ_c states, evolving from small, color transparent configurations to their asymptotic sizes. The measured J/ψ production cross sections in pA and AB collisions at SPS energies are consistent with both — purely hadronic — scenarios. The predicted rapidity dependence of J/ψ suppression can be used to discriminate between the two experimentally. The importance of interactions with secondary hadrons and the applicability of thermal reaction kinetics to J/ψ absorption are investigated. We discuss the effect of nuclear stopping and the role of leading hadrons. The dependence of the $\psi'/J/\psi$ ratio on the model assumptions and the possible influence of refeeding processes is also studied.

*Supported by the Alexander v. Humboldt Foundation

†Email: cspieles@lbl.gov

I. INTRODUCTION

Experimental data from the CERN SPS [1–4] clearly show that the yield of J/ψ-mesons in pA and AB collisions is suppressed when compared to hard QCD production. A substantial portion of these data can be described in simple models of nuclear absorption with certain assumptions about the dissociation cross sections, *e.g.* [5–13]. Recent, preliminary data on J/ψ production in Pb+Pb collisions [2–4] have generated an intense and ongoing controversy regarding the necessity of a novel suppression mechanism, *e.g.* a quark-gluon plasma [14], to explain the data or whether the suppression can be due to hadronic interactions. (For theoretical reviews, see Refs. [15–18].) Charmonium production and absorption has been studied first by means of semianalytical models of heavy ion collisions and/or thermal rate calculations [5–14,19–24] as well as, more recently, within microscopic hadronic transport models [25–30]. Some current models suggest purely hadronic explanations of the suppression while others claim that this is not possible. Here we use different model scenarios to identify crucial theoretical and experimental conditions which have to be met before definite conclusions can be drawn.

In simple analytical models of J/ψ suppression, based on a semiclassical Glauber approach, nuclear absorption is calculated by convoluting nuclear density profiles with an assumed cross section for dissociation by nucleons. The model parameters can generally be tuned to fit all pA data as well as all the AB data except Pb+Pb [6–13] . Absorption by produced hadrons, comovers, is typically also included in these models [7,9–13]. The comover dynamics is treated in a simple, schematic fashion, generally assuming that the comover density scales with the number of nucleon participants with the exception of Ref. [13]. It is not straightforward to distinguish between these results because of the variation of model parameters such as the comover dissociation cross sections, nuclear density profiles, formation and freeze-out times, as well as including feed-down to the J/ψ from more massive charmonium states. However, except for Ref. [13], all these studies claim that hadronic interactions alone cannot account for the J/ψ suppression in all pA and AB data.

Implicitly, geometrical models of nuclear absorption such as Glauber scattering assume that the nuclei traverse each other without distortion or energy loss. This seems to be appropriate for the description of the hard Drell-Yan [31,32] or $c\bar{c}$ [33] production processes and some authors also treat charmonium dissociation perturbatively [34]. However, the dissociation of charmonium need not necessarily be associated with a large momentum transfer. Therefore, nuclear absorption may result from soft processes which have been shown to dominate the charmonium dissociation at SPS energies [23]. If nuclear absorption is a soft process, the nucleons may scatter and lose energy before interacting with a charmonium state. Microscopic transport models, which approximate the soft hadron dynamics of a heavy ion collision as a cascade of binary scatterings, include this nontrivial baryon dynamics and are therefore adequate tools for the simulation of charmonium absorption. Moreover, they treat the complete space-time evolution of secondary hadrons in a consistent fashion.

However, the treatment of hard production processes as $gg \to c\bar{c}$ or $q\bar{q} \to \mu^+\mu^-$ is not obvious in the microscopic simulation of a soft hadronic cascade. The Drell-Yan production cross section in pA interaction is known to scale linearly with A [31,32]: $\sigma_{\rm pA} = \sigma_0 A$. Because of the apparent charmonium absorption discussed below there is no direct experimental evidence for linear scaling in charmonium production, or the hard nature of this process,

respectively. However, we assume hard production of charmonium since measurements of open charm production in $\pi + A$ reactions show no significant deviation from A scaling [33]. It should be mentioned, though, that the open charm data at low transverse momentum suffers from low statistics. We also note that, even though charmonium production does not scale as A, the exponent, 0.9 [35,36], is closer to unity than for lighter hadrons at low p_T and x_F which grow approximately as $A^{2/3}$ [37].

The near linear scaling of the $c\bar{c}$ production in pA reactions is a consequence of requiring a single perturbative parton-parton interaction. To simulate this microscopically, soft interactions of nucleons and the associated energy loss must be neglected. In Refs. [25,26], $c\bar{c}$ production was implemented into the hadronic transport code as a possible subchannel of the total NN cross section. This is certainly not consistent with the picture of perturbative $c\bar{c}$ production. In Ref. [28–30], on the other hand, the space-time production points are obtained from hard processes in each event before the hadronic background simulation. Charmonium dissociation is also treated differently in the various models. Some simulations, [26,28,29], assume that charmonium precursor states can be immediately dissociated by nucleons with constant cross sections larger than 5 mb. In Ref. [30] the charmonium cross sections evolve from small, color transparent states while Ref. [25] gives no definite formation time. Only Refs. [29,30] include feeddown from ψ' and χ_c mesons. Based on rather different model treatments of the charmonium dynamics and the interconnection of hard and soft processes, all these studies claim that conventional hadronic scenarios are consistent with the preliminary Pb+Pb data.

In this work, we simulate three different scenarios of charmonium absorption within the same calculational framework and compare the results. We apply the Ultrarelativistic Quantum Molecular Dynamics model v1.1 [38] for all calculations presented here.

In the first scenario, charmonium states are assumed to be produced as color-octet states which can be dissociated by nucleons only [11]. In the second scenario, nuclear absorption is treated in the same way as the first. However, secondary hadrons may dissociate the fully formed J/ψ, ψ' and χ_c states after a finite formation time. Finally, we investigate a scenario in which the charmonia are produced as distinct color-singlet states and evolve from small, color transparent configurations to their asymptotic sizes [23,30].

In Sec. II, the model framework and the distinct scenarios will be discussed in detail. The results of the simulations are then presented and discussed in Sec. III. In Sec. III A, we examine the consistency of transverse energy spectra measured by different experiments and compare them with our calculated distributions. In Sec. III B, some qualitative features of charmonium suppression and the space-time evolution of the system are discussed. Sec. III C compares the quantitative AB systematics of J/ψ suppression within our scenarios to the data. After a short discussion of the basic differences between semianalytical and microscopic descriptions of the comover dynamics in Sec. III D, we turn to the $\psi'/J/\psi$ ratio and its sensitivity to different model assumptions in Sec. III E. In Sec. III F, the dependence of J/ψ suppression on the projectile energy is studied. The key role of rapidity in discriminating between the different scenarios J/ψ suppression is identified in Sec. III G. Finally, we investigate the time dependence of J/ψ-comover collision energies and dissociation rates in Sec. III H. The applicability of thermal reaction kinetics is also discussed. In Sec. IV, we summarize our results and draw conclusions.

II. THE MODEL

A. The general framework

We simulate the production and the absorption of charmonium states in heavy ion collisions within the Ultrarelativistic Quantum Molecular Dynamics model [38]. This model has been shown to successfully describe final rapidity distributions of negatively charged hadrons and net-baryons in $p+p$ and nucleus-nucleus collisions [38]. While the model prescription for the charmonium rescattering stage is varied in order to study different conceivable scenarios, the initialization of the nuclei and the simulation of the hard $c\bar{c}$ production process are the same for all calculations presented in this work. The large number of parameters in the phenomenological microscopic model [38], especially in its collision term, have not been altered in the present study. The default values of these parameters are fit to data from elementary hadronic and p+A reactions over a range of energies. All concepts and parameters related to the treatment of heavy quarkonia in the model are specified in the following.

We apply perturbative QCD to the production of charmonium states by simulating nucleus-nucleus collisions in the impulse approximation. This is done microscopically by allowing freely streaming projectile and target nucleons to scatter without deflection or energy loss. The nuclear dependence of the parton distribution functions is neglected. The resulting space-time distribution of charmonium production points is inserted into the evolving hadronic environment calculated with UrQMD since the rare quarkonium production processes are only small perturbations on the heavy ion collision[1]. Our model is thus designed to account for partonic and hadronic aspects of the charmonium dynamics.

In UrQMD, the initialization of the projectile and target nuclei is based on the Fermi-gas ansatz. The centroids of the nucleons are then randomly distributed within a sphere of radius

$$R(A) = r_0 \left[\frac{1}{2}\left(A + \left[A^{1/3} - 1\right]^3\right)\right]^{1/3}, \tag{1}$$

[38]. The effective interaction radius is somewhat larger than $R(A)$ since the individual nucleons have a finite size. In pA reactions, a smeared out surface region of $\Delta R = 1.1$ fm, extending beyond $R(A)$, results from the geometrical NN cross section, $\sigma \approx 40$ mb. The parameter $r_0 = \left(\frac{3}{4\pi\rho_0}\right)^{\frac{1}{3}} = 1.14$ fm since the nuclear matter ground state density $\rho_0 = 0.16$ fm^{-3} is used in UrQMD. The above described initialization renders a good agreement with measured charge density distributions in nuclei [39].

We use this initialization procedure for the simulation of hard processes via perturbative QCD and the soft hadronic cascade, respectively. Consequently, the average nuclear density profiles are the same. However, in each event, the initial positions of the nucleons are determined independently for the two simulations after the impact parameter b is chosen. Thus,

[1]Since we consider only exclusive charmonium production, the QCD factorization theorem is inapplicable.

we insert the $c\bar{c}$ states into the hadronic environment according to an averaged distribution of hard production processes rather than linking the hard and soft simulations event by event. We therfore avoid strong and probably unphysical spatial correlations between hard and soft processes[2].

In the microscopic UrQMD transport model [38], many nucleons are excited to baryonic strings, *i.e.* their constituent quarks and diquarks are separated and propagate independently as the endpoints of color flux tubes. A significant fraction of the constituent quarks in the incident nucleons may thus appear as the core of leading mesons and are allowed to interact immediately after their production while leading baryons containing the remaining diquark interact with a reduced cross section in the UrQMD model. A sharp distinction between nuclear absorption and absorption by secondaries is not supported in this picture of nucleon break-up.

B. Distinct scenarios

We now introduce the scenarios for quarkonium suppression applied in our simulations.

1. Scenario I

This scenario follows Ref. [11]. Charmonium states are assumed to be produced as color-octet 'preresonance' states, $|c\bar{c}g\rangle$, which exist until after their passage through the nuclei is completed. These preresonance states can be dissociated by nucleons with a constant and universal cross section. In the NN center-of-mass frame, the $|c\bar{c}g\rangle$ states are produced at rest. Nuclear stopping and a change of the absorption cross section due to string excitation of incident nucleons is not considered. Then, in the UrQMD simulation, all but the charmonium-nucleon interactions have zero cross sections. J/ψ dissociation by secondary hadrons is not taken into account, since QCD calculations with heavy quarks predict a strong damping close to threshold [34]. There is one free parameter, the $|c\bar{c}g\rangle$–nucleon cross section.

2. Scenario II

According to this scenario, nuclear absorption is due to interactions of color-octet states. Thus, absorption by nucleons is calculated as in Scenario I, and the $|c\bar{c}g\rangle$ dissociation cross section is the first free parameter. Thus, we follow the arguments of [11] and the 'preresonance' hypothesis, respectively, as far as the nuclear absorption is concerned.

---

[2]If the hard and soft simulations are linked event by event, the resulting absorption probabilities sensitively depend on technical details of the implementation, *e.g.* whether the position of a produced J/ψ is chosen to be exactly the arithmetic mean of the positions of the two incident nucleons or randomly distributed between them. This seems to be unreasonable and is due to the naive geometrical interpretation of the interaction cross section in the semiclassical cascade.

Then, in a full UrQMD simulation, the environment of secondary hadrons is calculated. After their finite formation time (on average, $\tau_F \approx 1$ fm/c) resulting from the string fragmentation used in the UrQMD model, secondary hadrons may dissociate the J/ψ, ψ' and χ_c, which are assumed to be fully formed states by τ_F. In order to clearly separate the nuclear absorption of color-octet states from the delayed interactions of produced mesons with the asymptotic color-singlet states, we exclude the prompt interactions of leading secondary hadrons. The interaction of the leading quarks is effectively accounted for in the calculation of the nuclear absorption because the possible break-up of the incident nucleons due to a string excitation is ignored.

To calculate charmonium dissociation by secondary hadrons, it is necessary to distinguish between the distinct charmonium states in the simulation. The charmonium states are distributed according to their assumed production probability times their decay probability to J/ψ's. Thus 40% of the final states are χ_c's, 55% are J/ψ's, and 5% are ψ's [40]. According to the degeneracy of the angular momenta, 1/3 of the χ_c's are χ_{c10} states and 2/3 are χ_{c11} states. Their momenta are assigned according to the parametrization [41],

$$E\frac{d\sigma}{dMdp^3} \sim (1 - x_F)^{3.55} \exp(-p_T\, 2.08\, \mathrm{GeV}^{-1}) \; . \tag{2}$$

Unlike Ref. [11], we assume that the comover dissciation cross sections are predominantly nonperturbative at SPS energies, as shown for the dissociation by nucleons [23]. The nucleon absorption cross sections, $X(c\bar{c}) + N$, were derived in the framework of a nonrelativistic quarkonium model [23], obtaining $\sigma(J/\psi N) = 3.6$ mb, $\sigma(\psi' N) = 20$ mb, $\sigma(\chi_{c10} N) = 6.8$ mb, and $\sigma(\chi_{c11} N) = 15.9$ mb. These cross sections are not relevant for nuclear absorption in this scenario which is assumed to be exclusively due to interactions of the hypothetical color-octet states, as discussed above. The charmonium-meson cross sections ($X(c\bar{c}) + \pi$, $X(c\bar{c}) + \rho$, *etc.*) are obtained by scaling the nucleon absorption cross sections by a common factor F so that $\sigma(X(c\bar{c})M) = F\,\sigma(X(c\bar{c})N)$. In the additive quark model, $F = 2/3$. However, in this scenario it remains a second tunable parameter. Thus, additional suppression of the comover dissociation cross sections due to the relatively lower $X(c\bar{c}) + M$ collision energies can effectively be accounted for by adjusting F. All comover interactions above the respective dissociation thresholds are assumed to break up the charmonium state.

Charmonium dissociation is thus calculated in two different simulation modes for nuclear and comover absorption, respectively, assuming factorization of nucleon and comover absorption. Separate survival probabilities for dissociation by nucleons, S_N, and mesons, S_M, are computed. The total survival probability is then $S_T = S_N S_M$. There are similarities between this scenario and the two-stage cascade used in Ref. [29].

3. Scenario III

Here, the charmonium states are produced as distinct color-singlet states. Their dissociation cross sections evolve linearly from small, color transparent configurations [23]. Charmonium absorption is considered as a nonperturbative process, thus nuclear stopping is included in the calculation of nuclear absorption. In particular, nucleons which are excited to strings in a prior NN collision have a reduced cross section since they exist only as leading

diquarks during their formation time. Charmonium states can interact with incident nucleons, leading quarks and diquarks, and secondary hadrons (after their formation time). The production probabilities of the individual charmonium states and their momentum distributions are chosen as in Scenario II. The rescattering cross sections for $X(c\bar{c}) + B$, assuming $B \equiv N$, are taken from Ref. [23] (see Scenario II). We now let $F = 2/3$ according to the additive quark model. All baryon and meson collisions above the respective dissociation thresholds are assumed to break up the charmonium state. The cross sections correspond to the geometrical transverse radii $r_T^i = \sqrt{\frac{\sigma^i}{\pi}}$ of the charmonium states. We use σ^i to estimate the respective formation times τ_F^i of the charmonium states by choosing $\tau_F^i = r_T^i/c$. During these formation times the cross sections increase linearly with t [23], starting from $\sigma_0 = 0$ at $t = 0$. Since all the parameters have been fixed either by prior model calculations [23] or the dynamical model, UrQMD, itself, we do not adjust any parameters in this scenario.

III. RESULTS AND DISCUSSION

A. E_T distributions

The transverse energy distributions in different systems at SPS energies have been calculated with the UrQMD model [38]. Figure 1 shows the differential cross section of the transverse energy produced in Pb(160 GeV)+Pb collisions within the pseudorapidity range $2.1 < \eta < 3.4$. The UrQMD result is compared with experimental data from the NA49 Collaboration [42]. The overall agreement appears to be good although the detailed shape of the spectrum at very central events, *i.e.* very high E_T, is somewhat different. This difference may be due to statistical limitations of the simulation since we have analyzed only 1000 events. The disagreement between model and experiment at very low E_T can be due to an impact parameter cut at $b = 12.5$ fm in the calculations which leaves out part of the very peripheral reactions. The comparison between the S(200 GeV)+Au data from the NA35 Collaboration and the model calculation within the same acceptance, $2.1 < \eta < 3.4$, shows an agreement of similar quality, see Fig. 1.

The hard collision spectrum of neutral E_T for Pb(160 GeV)+Pb and S(200 GeV)+U reactions has also been calculated, based on the following concept: First, the number of hard nucleon-nucleon collisions, which is proportional to the yield of Drell-Yan muon pairs, is determined microscopically in the simulation of freely streaming nucleons, as described in Sec. II A. The associated simulation of all soft processes with the full hadronic cascade, initialized with the same impact parameter b, then renders the information about the produced transverse energy.

Figure 2 (a) shows the number of Drell-Yan muon pairs ($\propto$ number of collisions in the simulation of hard processes) in Pb+Pb interactions as a function of the produced neutral transverse energy within $1.1 < \eta < 2.3$. The normalization is arbitrary. Experimental data from NA50 [43] have been put on the plot as well. However, the abscissa has been rescaled since the most recent data [4] indicate that the absolute E_T values of the previous publications on Pb+Pb collisions [3,43] have shifted. We are aware that the new analysis does not imply a simple overall linear rescaling of the old data points. However, in order to reasonably compare the gross features of the experimental dimuon E_T spectrum with our model calculation, we have multiplied all E_T-values of the data in the plot by 0.8. This

value was estimated by comparing the $E_T - E_{ZDC}$ contour plots of the Tsukuba '97 [43] and the Moriond '98 [4] proceedings. The UrQMD simulation seems to be in rough agreement with the resulting dN/dE_T spectrum. The agreement between the model and experiment is not unexpected since the production of the NA49 transverse energy had been shown to be correctly described. The additional free streaming simulation is very simple and represents a well understood model of hard scattering processes in nucleus-nucleus collisions.

The agreement between model and experiment (NA38) [1,44] seems to become poor in the case of the asymmetric S+U system, see Fig. 2 (b). The UrQMD calculation appears to significantly overestimate the neutral transverse energy within $1.7 < \eta < 4.1$ although the E_T spectrum of the similar S+Au system agrees with the NA35 data, as was shown in Fig. 1. Note that the use of a model for the simulation of hard collisions and the weighting of the E_T distribution with the respective number of Drell-Yan dimuons affects only the *shape* of the E_T spectrum as compared to a normal distribution of all events — central events are favored, since they correspond to a higher number of nucleon-nucleon collisions. Thus, even if the correlation between transverse energy and impact parameter was completely wrong in UrQMD, which seems unlikely given the agreement in Fig. 1, this would merely lead to an incorrect weighting of the respective E_T values. In Fig. 2 (b), however, one sees that the *maximally achievable* neutral transverse energy differs by about 25%.

In view of our simulation results, the NA38 neutral transverse energy spectrum of S(200 GeV)+U seems to be inconsistent with the transverse energy spectrum of S(200 GeV)+Au measured by NA35. On the other hand, the (rescaled) NA50 Pb+Pb spectrum appears to be consistent with the NA49 and the NA35 spectrum. Given the consistency of the microscopic simulation with three different experimental measurements we assign the remaining discrepancy in S+U to a possible problem in the determination of the NA38 E_T scale. In order to compare our calculations of J/ψ production as a function of E_T with NA38 data, we will therefore apply a scaling factor of 1.25 to the E_T values reported by NA38 [1,44].

B. Space-time picture of charmonium production and absorption

In this section, we illustrate how charmonium production and absorption is incorporated into UrQMD. Figs. 3 (a)-(d) visualize the production and absorption points of $c\bar{c}$ states in the z-t plane for central Pb(160 GeV)+Pb collisions as calculated with UrQMD. For this qualitative analysis, time independent baryon and meson absorption cross sections have been used. Their absolute value is irrelevant for this discussion. The impact of a time dependence of the cross sections on the dissociation probabilities will be discussed later in this section.

The straight lines indicate the light cone trajectories of the geometrical boundaries of the nuclei. Hard production processes occur only at times and positions where the nuclear densities of projectile and target actually overlap in the course of the evolution. Since the nuclei traverse each other without energy loss in the present simulation of hard processes, the overlap region is determined by the light cone bands in the plot. Figure 3 (a) shows the $c\bar{c}$ production points. They all lie in the nuclear overlap region. Figure 3 (b) shows the points of $c\bar{c}$ dissociation by 'hard nucleons' in the z-t plane, *i.e.* nuclear stopping is not included in the simulation of nuclear absorption. Therefore, nuclear absorption is constrained to the region covered by the light cone bands of the two nuclei, however not to the actual overlap

region of both bands. The charmonium states are produced at rest. Therefore, the spatial distribution of absorption points must coincide with the distribution of production points, *i.e.* it is restricted to its longitudinal range $|z| < 0.8$ fm. The temporal distribution of $c\bar{c}$ dissociation, however, naturally exhibits some delay as compared to the production, since absorption does not take place instantaneously.

Fig. 3 (c) shows the points of $c\bar{c}$ dissociation by nucleons as in Fig. 3 (b), but the charmonium states are now produced according to their assumed momentum distribution given by Eq. (2). Therefore, the spatial coordinates of production and absorption do not coincide. However, due to their high mass, few charmonium states actually acquire velocities high enough to propagate for very long and still be within reach of the nuclei which did not suffer energy and velocity loss in this calculation.

Fig. 3 (d) shows the points of $c\bar{c}$ dissociation by 'soft nucleons' in the z-t plane, *i.e.* nuclear stopping is included in this simulation of nuclear absorption. Nuclear absorption can therefore occur anywhere within the forward light cones of the two nuclei. Most of the nuclear dissociation processes, however, take place at very early times, $t \lesssim 3$ fm/c.

Fig. 4 (a) shows the points of $c\bar{c}$ dissociation by mesons in the z-t plane for central Pb(160 GeV)+Pb collisions. Note that mesons containing a constituent quark of an incident nucleon are included in this plot. These leading hadrons can interact with other particles instantaneously, however, their cross section is reduced by a factor of two. Most of the absorption processes within the first 1.5 fm/c are due to interactions with leading mesons. To demonstrate this, Fig. 4 (b) shows the points of $c\bar{c}$ dissociation by mesons in the z-t plane, where only interactions of fully formed mesons are taken into account. Clearly, if leading mesons are considered as comovers, they dominate the comover absorption probability. Even a strong damping of the dissociation cross section close to threshold [34] would not justify neglecting these processes, since they occur well above threshold (see Sec. III H). On the other hand, nuclear stopping reduces the nuclear absorption considerably. This is due to the fact that when a nucleon is excited into a string, it loses one of its constituent quarks which becomes part of a leading meson. Accordingly, the dissociation cross section of the baryon containing the remaining leading diquark is rescaled to 2/3 of the nuclear absorption cross section in the UrQMD simulation.

C. AB systematic of J/ψ suppression

Here we discuss the systematics of J/ψ production and suppression as a function of AB in our three scenarios. We compare our results to the data from several projectile-target combinations: p(450 GeV)+C, p(200 GeV)+Cu, p(200 GeV)+U, S(200 GeV)+U, and Pb(160 GeV)+Pb. The 450 GeV and 160 GeV simulations are rescaled to $p_{lab} = 200$ GeV with the parametrization of Ref. [45], as done by NA50 [2,3].

1. Scenario I

Figure 5 shows a comparison between the semianalytical Glauber calculations of Kharzeev *et al.* [11] and UrQMD/Scenario I using the same absorption cross section,

$\sigma^{\rm diss} = 7.3$ mb. The experimental data are also shown [3]. The J/ψ, ψ' and χ_c are assumed to interact with nucleons while in $|c\bar{c}g\rangle$ color-octet states.

Charmonium dissociation by secondaries is assumed to be negligible. As in the geometrical picture, the $c\bar{c}$ states are produced at rest and the nuclei traverse each other without energy loss. Nucleons do not suffer a reduction of their cross section due to string excitations. The difference between the semianalytical model and the microscopic simulation according to Scenario I is 10% in S+U collisions ($S_{\rm Glauber} = 0.49$ vs. $S_{\rm UrQMD} = 0.45$). This is due to the different nuclear density profiles: In Ref. [11] a Woods-Saxon shape is used, whereas UrQMD initializes hard spheres with an effectively smeared-out surface layer due to the finite geometrical NN cross sections, see Sec. II A. Note that the cross sections are derived by multiplying the respective survival probabilities with the experimental $p+p$ cross section [3]. In Ref. [11], p+D reactions have been used as reference value for determining the nuclear absorption cross section. Surprisingly, the p+D point is above the $p+p$ point, measured at the same energy. Note that Fig. 5 is not our best fit through the pA and S+U data. As in Ref. [11], the present (analogous) calculation underpredicts the J/ψ absorption in Pb+Pb, while reasonable agreement for all other systems is achieved. However, a value of 9 mb for the color-octet absorption cross section yields an acceptable simultaneous agreement with all data if the $p+p$ cross section is left as a free parameter, as shown in Fig. 6. Note that our $p+p$ value differs from the data by two standard deviations in this case.

2. Scenario II

Figure 7 shows a calculation of the J/ψ systematics within Scenario II. Recall that in order to avoid an overlap between the interactions of the charmonia as color-octet and color-singlet states, leading mesons are not allowed to interact. The early stage of $c\bar{c}$ absorption is thus described solely by Glauber-like nuclear absorption using a universal color-octet dissociation cross section, $\sigma(X(c\bar{c})N) = 4.8$ mb, *cf.* [7]. Interactions with secondary hadrons occur only after their formation time — on the average $\tau_F \approx 1$ fm/c — after the charmonium states have fully formed. For the comover absorption cross sections we take $F = 0.5$ with the nucleon absorption cross sections from Ref. [23]. The calculated J/ψ production cross sections for the given parameter values all lie within the experimental error bars. The measured cross sections are therefore consistent with a purely hadronic picture of the dynamics as described by Scenario II. Note that similar model assumptions in a different hadronic cascade model with a somewhat different choice of parameters have lead to the same conclusion [29]. Semianalytical calculations, however, employing the same nuclear dissociation cross section [12] fit the S+U data with significantly smaller comover absorption cross sections. In contrast to the microscopic calculation presented here, simultaneous agreement with the Pb+Pb data cannot be achieved in that analysis, as will be discussed in Sec. III D.

3. Scenario III

Figure 8 shows the UrQMD calculation assuming the charmonium states are produced as color-singlet states and evolving from small, color transparent configurations. Nuclear stopping and dissociation by leading diquarks and quarks is taken into account. One observes

a fair agreement of the simulation with the AB systematics of the data. The measured cross sections are therefore also consistent with a purely hadronic system. Note that no parameters were tuned to fit the data.

Figure 9 shows the resulting E_T distributions for the ratio of J/ψ to Drell-Yan production in Pb+Pb and S+U reactions. The gross features of the E_T dependencies of the ratios are reasonably well described by the model calculations. In particular, the calculated result is smooth in both cases, without abrupt discontinuities, in agreement with new high statistics data comparing J/ψ production to the minimum bias cross section [46]. Apparent discontinuities in the preliminary data which compared the more abundant J/ψ to limited statistics Drell-Yan production had been interpreted by some as a sudden onset of a deconfined phase [8,47,48].

We want to point out that possible agreement or disagreement of the simulation with the final data depends decisively on the determination of the correct E_T scale. When dealing with preliminary data, horizontal error bars indicating the systematic uncertainties in the E_T scale of the experimental analysis would be helpful. The uncertainties of the E_T determination in our calculation are only statistical and lie within the bin width of the histograms.

Note that the slight underestimation of the J/ψ over Drell-Yan production at low E_T seen in Fig. 9 can be related to an overestimation of the Drell-Yan cross section at low E_T, visible in Fig. 2 (a). Calculations in the context of the Dual Parton Model also show have feature [13].

D. Semianalytical vs. microscopic descriptions

It has been shown in the previous analysis that, within the microscopic hadronic transport model UrQMD, comover interactions can explain the observed J/ψ suppression in S+U and Pb+Pb collisions. The question then naturally arises why semianalytical calculations of charmonium production and absorption, based on the Glauber approach and the wounded nucleon model, cannot also simultaneously describe these data [10,12]. Therefore, it is worthwhile to examine some basic differences in the comover dynamics of the two approaches.

First, transverse expansion is neglected in the semianalytical models [10–13] although it is a feature of the true reaction dynamics, as established experimentally [49]. However, the full system including the transverse dynamics [50] is treated explicitly in microscopic models like UrQMD. It remains to be seen how the J/ψ survival probabilities are quantitatively affected by the inclusion of a realistic transverse expansion in the semianalytic models.

Secondly, comover scenarios based on the wounded nucleon model assume a linear scaling of the produced hadron rapidity densities with the number of participants, $E\mathrm{d}^3N/\mathrm{d}p^3 \sim N_{\mathrm{part}}^{\alpha}$ where $\alpha = 1$. In contrast, a possible enhancement of the meson yield at midrapidity for nuclear collisions relative to N+N collisions has been observed [51]. The h^- yield per participant nucleon pair, extrapolated to full phase space, is 4.0 ± 0.2 for Pb+Pb, compared to 3.6 ± 0.2 for S+S [52]. Measurements of the neutral pion production in Pb+Pb collisions as a function of centrality show that the pion yield in the interval $0.5 < p_T < 3$ GeV/c scales like $N_{\mathrm{part}}^{1.3}$ [53]. Thus, experimental observations suggest deviations from the simple assumptions of the wounded nucleon model at SPS energies. This is not surprising since measured particle momentum correlation patterns are in striking contrast to simple $p + p$

and $p + A$ extrapolations due to additional meson-meson and meson-baryon interactions in nucleus-nucleus collisions [54].

In UrQMD simulations of central Pb+Pb relative to central S+U collisions the meson yield scales like $N_{\rm part}^{1.25}$. This nonlinear scaling with the number of participants naturally explains at least a part of the "additional" suppression in the heavier system. Note that semianalytical studies where the comover densities have been extracted from the Dual Parton Model, which also exhibits a nonlinear scaling, produce simultaneous agreement with the S+U and Pb+Pb data [13].

Finally, semianalytic models generally neglect the considerable rapidity asymmetry of hadron production in asymmetric nuclear collisions [55] while UrQMD simulations also show this feature of the measured particle distributions. Even if the yields of produced hadrons over 4π scaled exactly with the number of participants, the relative comover densities extracted from the wounded nucleon model would be incorrect in the finite experimental acceptance cut of NA50 , $0 < y < 1$. According to the UrQMD simulation of central nuclear collisions, $\frac{N^{h^-}(\text{Pb+Pb})}{N^{h^-}(\text{S+U})}|_{0<y<1} / \frac{N^{h^-}(\text{Pb+Pb})}{N^{h^-}(\text{S+U})}|_{4\pi} = 1.12$.

E. The ψ' to J/ψ ratio

Figures 10 and 11 show the $\psi'/J/\psi$ ratio in pA and AB collisions as a function of AB. UrQMD calculations in Scenarios II and III are compared with the experimental data [2,56]. The observed weak A dependence of the ratio in pA reactions is consistent with the hypothesis of the formation of a 'preresonance' state, *e.g.* [11]. If the charmonium states are initially produced in the $|c\bar{c}g\rangle$ configuration and color neutralization takes sufficiently long, the produced J/ψ's and ψ''s are equally suppressed by nuclear absorption. This is reflected in Fig. 10, showing the calculations within Scenario II. In pA collisions, comover absorption is only a minor contribution to the total charmonium absorption. Consequently, the universal nuclear absorption cross section of the color-octet states results in a constant $\psi'/J/\psi$ ratio.

In Scenario III, the absorption cross sections for the individual charmonium states evolve linearly with time. Thus, the ψ', χ_{c10} and χ_{c11} states have absorption cross sections similar to that of the J/ψ as long as $\tau^i < \tau_F^{J/\psi}$. Only for $\tau^i > \tau_F^{J/\psi}$ the cross sections differ strongly, because then $\sigma(J/\psi N)$ has reached its asymptotic value while the cross sections of the larger resonances still increase. The differences in the calculated J/ψ and ψ' survival probabilities for pA reactions, as shown in Fig. 11, are therefore mainly due to nuclear dissociation processes in the later stage of the reaction and interactions with secondaries. Even in pA reactions comover interactions are not negligible in Scenario III because leading mesons are taken into account.

Figures 10 and 11 also show the calculated $\psi'/J/\psi$ ratio in S+U and Pb+Pb reactions. In Scenario II, the $\psi'/J/\psi$ ratios in S+U and Pb+Pb reactions very roughly agree with the experimental values. In Scenario III, dissociation by mesons leads to an even stronger decrease of the $\psi'/J/\psi$ ratio in S+U and Pb+Pb collisions than seen in the data [2]. Although shortly after charmonium production the charmonium-comover dissociation cross sections are similar for all states, the kinematic threshold leads to different dissociation probabilities.

The $\psi'/J/\psi$ ratios in nucleus-nucleus collisions seem to favor Scenario II as compared

to Scenario III, although neither describes the data satisfactorily. However, the parameter space of the models has certainly not yet been fully explored. Moreover, for a complete understanding of the ratio, quantum interference effects [57] as well as refeeding processes such as $\pi J/\psi \to \psi'\pi$ [27,58] must be considered. As can be seen in Fig. 11, the ψ' survival probability in S+U collisions in Scenario III would need to be increased by more than 50% in order to agree with the experimental observations. To test the effect of refeeding, we have implemented the process $\pi J/\psi \to \psi'\pi$ in UrQMD with an energy independent cross section above the kinematic threshold, $E_{\rm th} = m_{\psi'} + m_\pi$. The refeeding cross section is assumed to have a time dependence like that of the nuclear and comover absorption cross sections. In this case, $\sigma_{\pi J/\psi \to \psi'\pi} = 7$ mb would increase the $\psi'/J/\psi$ ratio by 50%. This cross section seems unrealistically large because this exclusive channel σ is larger than the inclusive $\sigma(\pi\, J/\psi) = 2.4$ mb we have used elsewhere even though the mass threshold is larger than $\pi\, J/\psi \to D\,\bar{D}$. In order to further explore the effectiveness of possible ψ' refeeding processes, we have implemented the channel $MJ/\psi \to \psi' M$, where M stands for any meson species. Then the refeeding cross section must be $\sigma_{MJ/\psi \to \psi' M} = 3$ mb in order to increase the ψ' yield by 50%.

Finally, note that a change of the ψ' dissociation cross section alone evidently has a direct effect on the $\psi'/J/\psi$ ratio while the J/ψ survival probability itself is hardly affected. Therefore, in view of the theoretical uncertainties concerning charmonium dissociation cross sections and formation times it seems premature to draw definite conclusions from the model comparison presented here.

F. Pb+Pb at 160 GeV vs. 80 GeV

Since lowering the SPS beam energy has been discussed, it is worthwhile to check if such a change could distinguish between an evolving $c\bar{c}$ dissociation cross sections and a constant cross section. With a constant cross section, nuclear absorption should be insensitive to the γ factor, *i.e.* the Lorentz contraction, of the nuclei because the reduced path length is canceled by the enhanced density. There is no cancelation, however, in the case of evolving cross sections. In the limit of very high beam energies the nuclei become transparent for charmonium states despite the large nuclear density, since the absorption cross section is essentially zero immediately after production. Comover absorption, on the other hand, should increase with energy in both scenarios because the number of secondaries rises. However, the average comover velocity should be also enhanced which increases their average formation times in the center of mass frame counteracting the effect of increasing density. Thus for very high energies, disregarding leading hadrons, absorption by comovers must eventually become negligible due to the large formation times. In any case, the comover density and its time evolution varies with energy and can lead to different characteristic behaviours within the two scenarios.

We have compared the calculations with the standard choice of parameters for the calculation with constant cross sections, Scenario II, and the evolving cross sections, Scenario III. The resulting survival probabilities for minimum bias Pb+Pb collisions at $E_{\rm lab} = 160$ GeV and 80 GeV are presented in Table I. In fact, the calculated energy dependence of the nuclear absorption within the two scenarios behaves as anticipated. Dissociation by nucleons stays constant in Scenario II while it decreases with increasing beam energy in Scenario III.

The numerical results show that the comover absorption gets slightly stronger with increasing energy both for constant and evolving dissociation cross sections. The combined effects of absorption by baryons and mesons lead to a decrease of the J/ψ survival probability for 80 GeV as compared to 160 GeV in the case of evolving cross sections and an increase for constant cross sections. However, the relative change of the survival probability is only on the order of a few percent in both cases. Thus the experimental distinction between the two scenarios with the suggested change of beam energy is unlikely.

G. Rapidity dependence of J/ψ suppression

Another means by which the charmonium production mechanism might be determined is the study of the survival probability as a function of rapidity. We investigate pA interactions because absorption effects are limited to only one nucleus and comover suppression is significantly reduced in pA relative to AB collisions. A constant absorption cross section should be independent of rapidity while an evolving cross section should produce more absorption close to the target since the asymptotic state is more likely to interact inside the target.

Figure 12 shows the rapidity dependence of the J/ψ survival probability in p+U reactions at $E_{\rm lab} = 200$ GeV. The predictions of Scenario II and Scenario III are compared. The charmonium absorption is dominated by nuclear absorption in this system although comover interactions are not completely negligible, in particular in Scenario III, see Figs. 7 and 8. The scenario of a constant color-octet dissociation cross section leads to a constant rapidity dependence of the J/ψ survival probability because the effective path length of charmonium 'preresonance' states does not depend on their longitudinal velocity as long as $y_{X(c\bar{c})} > y_{\rm target}$. The assumption of evolving color-singlet states leads to an increasing survival probability with increasing rapidity. At forward rapidities, the larger γ factor of the charmonium states leads to an increased formation time in the NN center of mass frame. The evolution of the dissociation cross sections is therefore delayed. The charmonium states suffer effectively less absorption during the passage through the target nucleus. The reverse effect is limited by the asymptotic values of the absorption cross sections. Therefore, the J/ψ survival probability saturates at negative rapidities.

The experimental examination of the rapidity dependence in pA reactions is a very promising test of the production mechanism because of the very distinct behaviour of the J/ψ survival probability. It would be particularly interesting to carry out this experiment at about the same energy as the nuclear collisions studied by NA38 and NA50. Detailed analyses of existing experimental data on the x_F dependence of J/ψ production in pA reactions [35,36] should also be used to test the validity of different production mechanisms as done in Ref. [59]. There, it is also shown that the shape of the x_F dependence changes with energy. It is conceivable that a realistic scenario of charmonium production and absorption involves a superposition of color-singlet and color-octet contributions [59], however, the relative importance may well be energy dependent.

H. A closer look into interactions with secondaries

From the results presented in Sec. III C we conclude that the observed J/ψ production cross sections in pA and AB collisions can be explained in purely hadronic scenarios provided that secondary particles can effectively dissociate charmonium. In Scenarios II and III we have employed universal and energy independent[3] comover absorption cross sections for the individual $c\bar{c}$ meson states, see Fig. 13. Given the $X(c\bar{c})\,N$ cross sections [23], the size of the comover cross sections — with a reduction of $F = 1/2$ and $2/3$, respectively — are presumably of the right order, if similar collision energies are considered. However, calculations within the framework of short-distance QCD [34] show that J/ψ dissociation by hard gluons is strongly damped close to the kinematic threshold. Such a calculation is shown in Fig. 13 for the process $J/\psi\,\pi$. This would significantly increase the survival probability. However, the comover absorption would not be completely suppressed because of the feeding from the less bound χ_c and ψ' states. For example, the survival probability due to interactions with comovers in minimium bias Pb(160 GeV)+Pb collisions in Scenario II increases from $S_M = 0.61$ to $S_M = 0.69$ if the J/ψ itself cannot be dissociated by mesons. As a result, the total survival probability in this system would increase from $S_{tot} = 0.31$ to $S_{tot} = 0.35$.

Calculations of $J/\psi\,\pi$ and $J/\psi\,\rho$ dissociation cross sections in the framework of a meson exchange model also show a suppression at low energies even for the exothermic $J/\psi\,\rho \to D\bar{D}$ process [24]. The cross section for the dissociation by pions according to these calculations is shown in Fig. 13. Note that the inclusion of a form factor would further decrease the cross sections [24].

From phase space arguments alone, *i.e.* assuming an energy independent matrix element, one would infer an *enhancement* for low relative velocities in the incoming channel if the dissociation process is exothermic. Calculations of cross sections involving heavier mesons in the incoming channels within meson exchange models would render valuable information in order to estimate comover absorption probabilities. Also, a deeper understanding of the reactions involving the χ_c and ψ' states is needed.

In a chemically equilibrated environment at temperatures less than 300 MeV, the consideration of interactions with π's and ρ's might be sufficient to quantitatively estimate the total comover absorption. In any kind of thermal hadronic scenario, higher resonances are negligible due to the low density, $\rho_H \sim \exp(-m_H/T)$. However, Table II shows the relative importance of the mesons which contribute most to J/ψ dissociation according to the nonequilibrium UrQMD calculation. Scatterings of the J/ψ's with π's and ρ's are indeed the dominant dissociation processes. However, together they are responsible for only about 40% of the total comover absorption. The composition is similar in Scenarios II and III. Twenty channels are left out of Table II, each of them contributing $\approx 1\%$ or less. However, they account for about 15% of the total absorption.

The string fragmentation scheme employed in UrQMD [38] determines the relative abundancies of hadron states in the nonequilibrium simulation. The choice of parameters is far from unique since the model can be compared to data only for experimen-

[3]Above the respective kinematic dissociation threshold, *i.e.* $\sigma_{\rm diss}(\sqrt{s}) = \theta(\sqrt{s} - E_{\rm th})\sigma_0$.

tally identifiable hadrons. In UrQMD, all states of eight different meson multiplets ($J^{PC} = 0^{-+}, 0^{++}, 1^{--}, 1^{+-}, 1^{++}, 2^{++}$ plus two excited 1^{--} multiplets) may be populated in a string fragmentation process. The probability to form a meson from one of these multiplets is chosen to be proportional to the spin degeneracy and inversely proportional to the average mass of the multiplet [38].

In Fig. 14, the average $J/\psi\,\pi$ collision energies as functions of time are shown for three different scenarios: constant cross sections including interactions of leading mesons (*cf.* Ref. [60]), constant cross sections excluding leading mesons (Scenario II), and evolving cross sections sections including interactions of leading mesons (Scenario III). We studied central Pb(160 GeV)+Pb collisions. All model simulations yield high average collision energies of $\langle E \rangle \approx 4.8$ GeV at $t \approx 1$ fm/c. As stated in Ref. [60], these collision energies are not compatible with an equilibrated hadron gas scenario since they correspond to a meson gas with a temperature of $T \approx 750$ MeV. The collision energies and the scattering rates at later times, $t > 2$ fm/c, are both consistent with temperatures of $T = 140 \pm 20$ MeV [60], thus allowing for the application of a thermal reaction kinetics model.

An important difference between the three scenarios presented in Fig. 14 is shown in Fig. 15 which determines the impact of the highly nonthermal secondaries at early times on the total comover absorption. The scattering rate as a function of time, normalized to one J/ψ-meson collision, is depicted. It can be seen that at early times $t < 2$ fm/c, dissociation by comovers is almost exclusively due to interactions of leading mesons. Moreover, if leading meson interactions are taken into account, they clearly dominate the total comover absorption. This is true for the scenario with constant as well as with evolving cross sections. Note that the dissociation cross section of a leading meson is only 1/2 of that of a fully formed meson. As can be seen from Figs. 14 and 15, the applicability of thermal momentum distributions for the comover-charmonium interactions in heavy ion collisions depends heavily on the underlying model assumptions. A thermal comover model seems to be a reasonable approximation in Scenario II while it cannot be justified in Scenario III where leading mesons are included.

Figure 16 shows the time integrated collision spectrum of $J/\psi\,\pi$ interactions in central Pb(160 GeV)+Pb reactions according to the UrQMD simulations. The high energy tails of the spectra calculated within the different model scenarios reflect the interactions at early times. They correspond to temperatures of $T \gg 300$ MeV. However, it is also clear from Fig. 16, that for all presented scenarios, more than 75% of $J/\psi\,\pi$ interactions occur at collision energies below 4.25 GeV. Thus, the threshold behaviour of all involved dissociation channels will finally decide, whether comover absorption is effective enough to explain the suppression of charmonium yields in nuclear reactions.

IV. CONCLUSIONS

We have studied the production and absorption of charmonium states at SPS energies using a microscopic hadronic model, UrQMD. The model simultaneously reproduces the final rapidity distributions of produced hadrons and net-baryons in pp and AB collisions. The simulations also agree with the measured total transverse energy spectrum for S(200 GeV)+Au (NA35) and Pb(160 GeV)+Pb (NA49) as well as with the E_T dependence of the Drell-Yan muon pairs in Pb(160 GeV)+Pb (NA50). At the same time the calcu-

lations are in significant disagreement with the S(200 GeV)+U E_T dependence of dimuon production (NA38).

Our study shows that nuclear absorption alone cannot yield prefect agreement with all measured J/ψ cross sections in pA and AB collisions at SPS energies. This is in accord with the findings of previous studies with semianalytical models. However, we find that a global fit to the AB systematics with a nuclear absorption cross section of 9 mb is not yet completely ruled out by the data taking into account its systematic and statistical errors and its in part still prelimary status.

The UrQMD model renders better agreement with the J/ψ data if comover dissociation is included and the charmonium is produced in color-singlet states which evolve in time. In this case, all parameters were fixed by other data before comparison to the NA50 data. The E_T dependence of the J/ψ/Drell-Yan ratio is also reproduced in this model. The $\psi'/J/\psi$ ratio agrees with the pA data, while the ψ' suppression in S+U and Pb+Pb is overestimated. Assuming produced color-octet states with a time independent, universal cross section and comover absorption of the fully formed $c\bar{c}$ states, yields equally good agreement with the J/ψ data. The overall trend of the $\psi'/J/\psi$ systematic for different projectile and target combinations is fairly well reproduced, although significant quantitative deviations from the data are found in nuclear collisions.

The rapidity dependence of the J/ψ survival probability in pA reactions is a promising observable by which the contributions of color-singlet and color-octet states to nuclear absorption processes can be disentangled.

The effectiveness of charmonium dissociation by interactions with secondaries is apparently crucial for the understanding of the experimental data in hadronic scenarios. The microscopic simulation shows that the charmonium-comover interactions are not close to an equilibrium situation. Heavy meson resonances contribute to a large fraction of all charmonium-comover interactions. The calculation of energy dependent cross sections for a large number of possible hadronic dissociation channels is a prerequisite for a quantitative understanding of comover absorption.

TABLES

TABLE I. Comparison of J/ψ survival probabilities for minimum bias Pb+Pb collisions at different energies for constant and evolving dissociation cross sections, *i.e.* Scenario II and Scenario III, respectively.

$E_{\rm lab}$	S_B^{II}	S_M^{II}	S_{tot}^{II}	S_B^{III}	S_M^{III}	S_{tot}^{III}
160 GeV	0.51	0.61	0.31	0.57	0.49	0.33
80 GeV	0.51	0.64	0.33	0.50	0.51	0.32

TABLE II. Contributions of different meson species to the total J/ψ comover absorption in central Pb+Pb collisions at 160 GeV according to the UrQMD simulation with Scenario II and III. The percentage of comover absorption due to the most dominant channels are shown.

Species	Scenario II	Scenario III
π	19.7 ± 0.3	18.6 ± 0.3
ρ	20.8 ± 0.4	18.6 ± 0.3
K	11.6 ± 0.3	11.1 ± 0.3
$K^*(892)$	8.9 ± 0.3	8.1 ± 0.2
η	5.4 ± 0.2	6.4 ± 0.2
ω	8.4 ± 0.3	6.3 ± 0.2
$a_2(1320)$	3.1 ± 0.1	4.4 ± 0.2
$a_1(1260)$	2.6 ± 0.1	4.2 ± 0.2
$b_1(1235)$	3.6 ± 0.2	3.8 ± 0.2
$a_0(980)$	3.0 ± 0.1	2.9 ± 0.1
Sum:	87.1 ± 0.8	84.4 ± 0.7

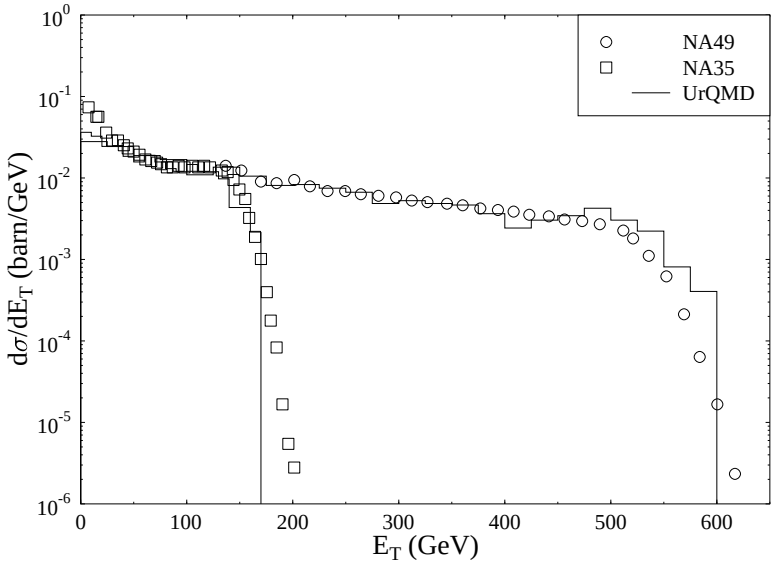

FIG. 1. Differential cross section of the transverse energy produced in Pb(160 GeV)+Pb and S(200 GeV)+Au collisions within the pseudorapidity range $2.1 < \eta < 3.4$. The UrQMD results are compared with data from [42].

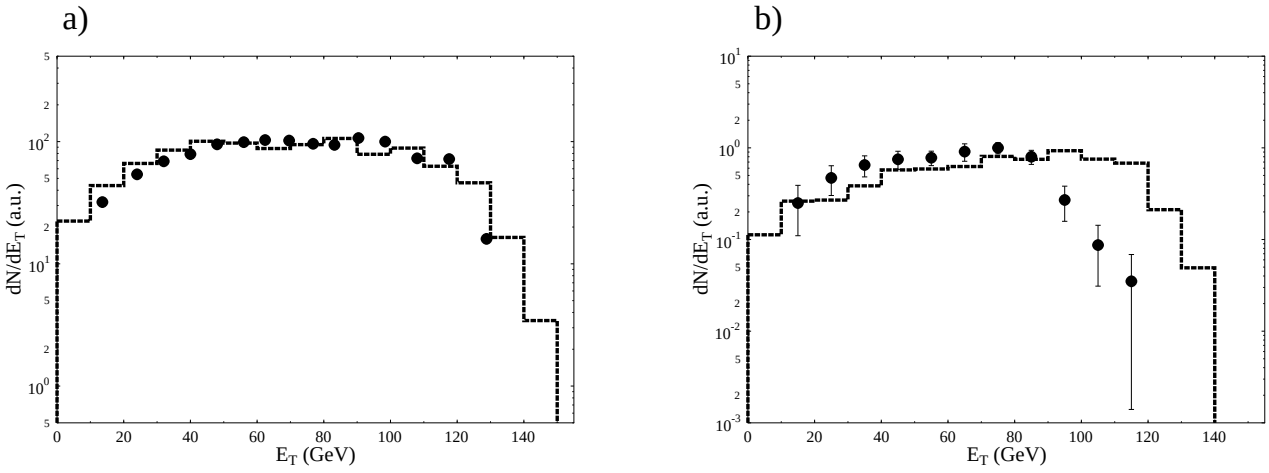

FIG. 2. a) Number of Drell-Yan muon pairs in Pb+Pb as a function of the produced neutral transverse energy within $1.1 < \eta < 2.3$ with arbitrary normalization. The UrQMD result is shown with data from NA50 [43] where the E_T-axis of the data is rescaled by 0.8. The modification is motivated by the recently published $E_T - E_{ZDC}$ contour plot [4] compared to the previously published analysis [43,3]. b) Number of Drell-Yan muon pairs in S+U as a function of the produced neutral transverse energy within $1.7 < \eta < 4.1$ with arbitrary normalization. The UrQMD result and data from NA38 [44] are shown.

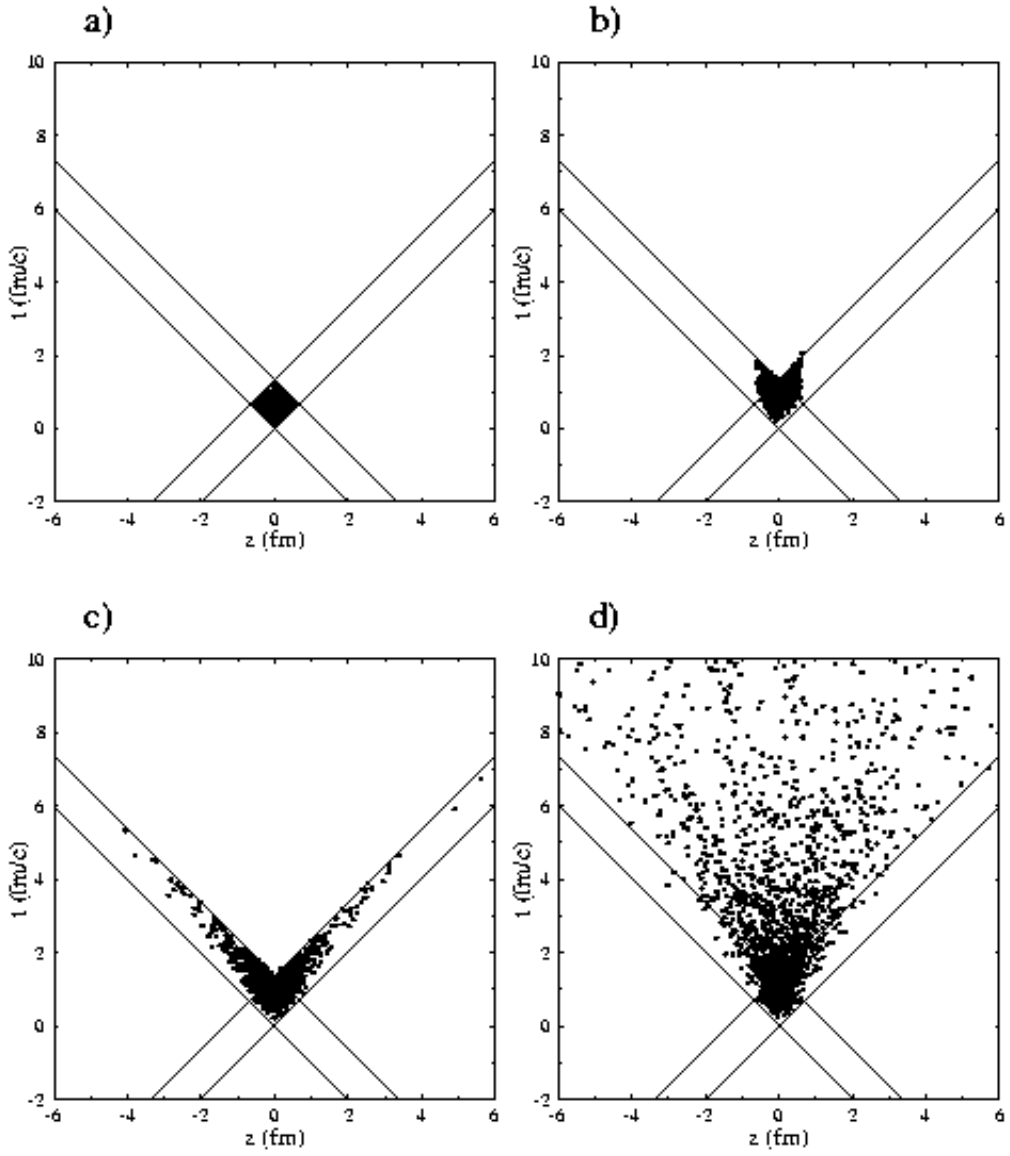

FIG. 3. Time evolution of a central Pb+Pb collision at $E_{\rm lab}$ = 160 GeV according to the UrQMD simulation with time independent absorption cross sections. The interaction points of charmonium states in the z-t-plane are shown. a) The $c\bar{c}$ production points. b) The $c\bar{c}$ dissociation points due to interactions with nucleons, if the momentum distribution of the charmonium states and the nuclear stopping is neglected. c) The momentum distribution of the charmonium states is now included while the nuclear stopping is still neglected. d) The momentum distribution of the charmonium states and nuclear stopping is taken into account.

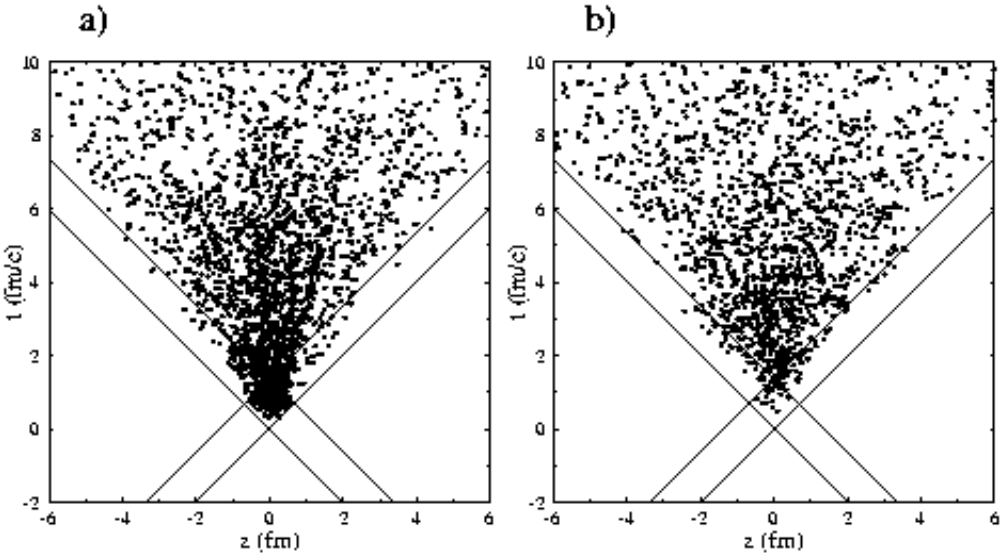

FIG. 4. Time evolution of a central Pb+Pb collision at $E_{\rm lab} = 160$ GeV according to the UrQMD simulation with time independent absorption cross sections. The interaction points of charmonium states in the z-t-plane are shown. a) The $c\bar{c}$ dissociation points due to interactions with mesons including leading hadrons. b) The $c\bar{c}$ dissociation points due to interactions with mesons without leading hadrons.

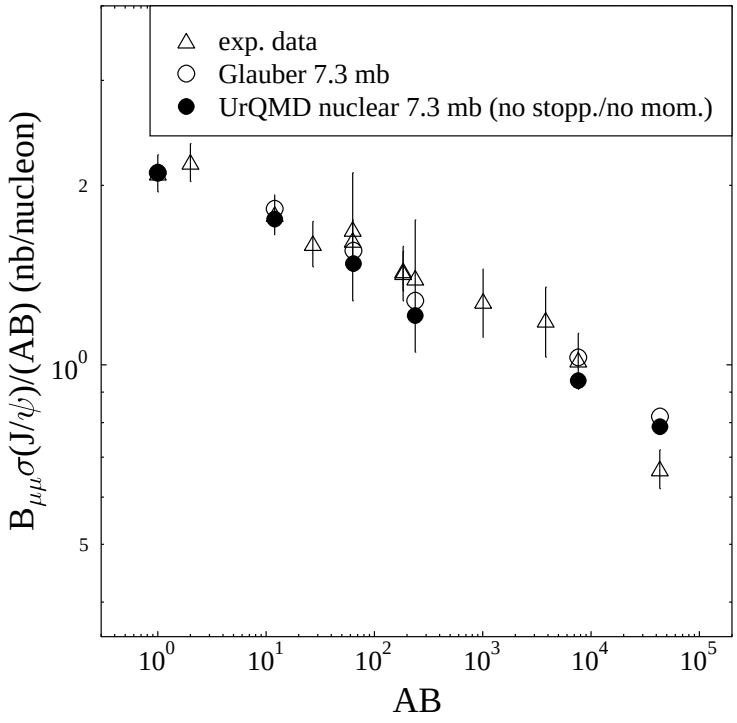

FIG. 5. J/ψ-production cross sections times dimuon branching ratio in the kinematical domain $0 < y_{cm} < 1$ and $|\cos\theta_{CS}| < 0.5$, and rescaled, if necessary, to $p_{\rm lab} = 200$ GeV as a function of AB. Open circles denote the semi-analytical Glauber calculations of [11] while the results of the microscopic UrQMD simulation without nuclear stopping and momentum distribution of the J/ψ, Scenario I, are shown as full circles. A universal and constant absorption cross section of $\sigma = 7.3$ mb is used for both. The data (open triangles) are from [3].

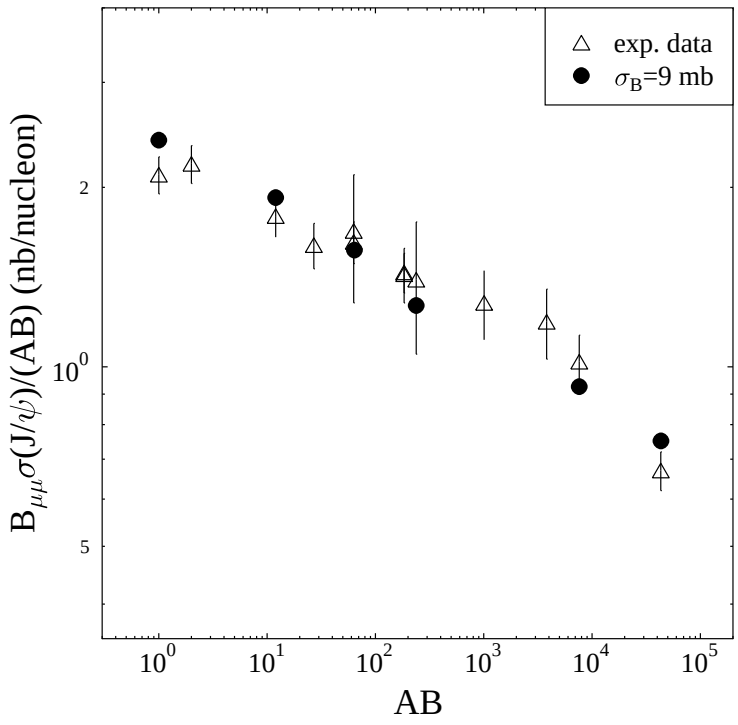

FIG. 6. J/ψ-production cross sections times dimuon branching ratio in the kinematical domain $0 < y_{cm} < 1$ and $|\cos\theta_{CS}| < 0.5$, and rescaled, if necessary, to $p_{\rm lab} = 200$ GeV as a function of AB. The results of the microscopic UrQMD simulation without nuclear stopping and momentum distribution of the J/ψ, Scenario I, are shown as full circles. A universal and constant absorption cross section of $\sigma = 9$ mb is used. The J/ψ production cross section in p+p reactions (the absolute normalization) is arbitrarily chosen. The data (open triangles) are from [3].

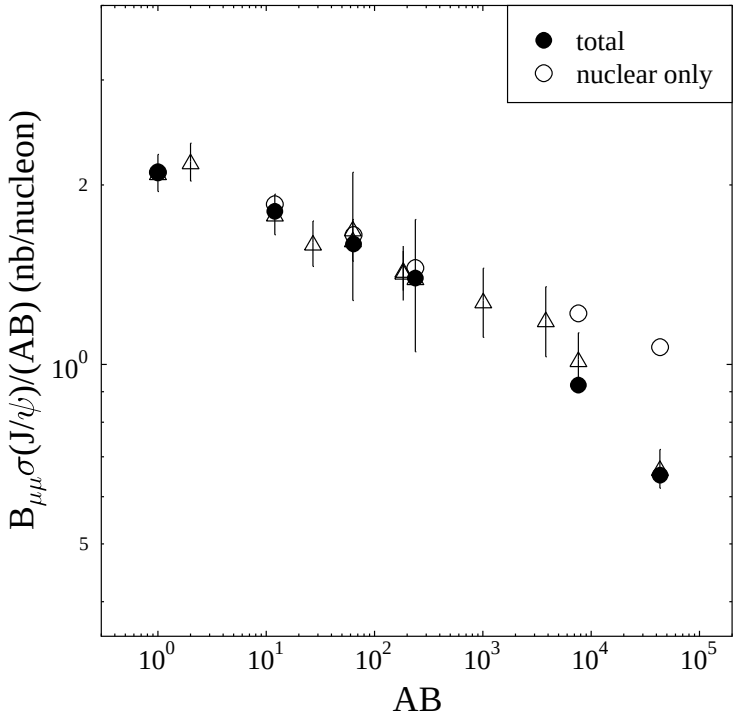

FIG. 7. J/ψ-production cross sections times dimuon branching ratio in the kinematical domain $0 < y_{cm} < 1$ and $|\cos\theta_{CS}| < 0.5$, and rescaled, if necessary, to $p_{\rm lab} = 200$ GeV as a function of AB. Full circles denote the results according to Scenario II. Nuclear absorption is calculated without stopping using a universal dissociation cross section of $\sigma = 4.8$ mb, *cf.* Ref [12]. Comover absorption is calculated in a full UrQMD simulation without leading hadrons. The charmonium-meson cross sections ($X(c\bar{c}) + \pi$, $X(c\bar{c}) + \rho$, *etc.*) are reduced by a factor of 1/2 from the cross sections for $X(c\bar{c}) + N$ from Ref. [23]. Open circles denote the production cross sections if only nuclear absorption is considered. The data (open triangles) are from [3].

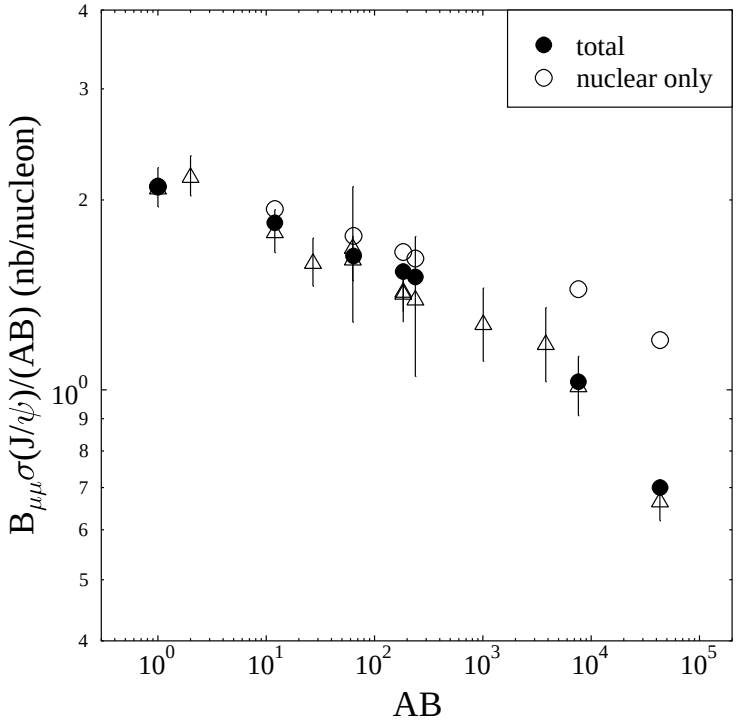

FIG. 8. J/ψ-production cross sections times dimuon branching ratio in the kinematical domain $0 < y_{cm} < 1$ and $|\cos\theta_{CS}| < 0.5$, and rescaled, if necessary, to $p_{\rm lab} = 200$ GeV as a function of AB. The UrQMD calculation with evolving dissociation cross sections, Scenario III, is shown. Open circles denote the production cross sections if only nuclear absorption is considered. The data (open triangles) are from [3].

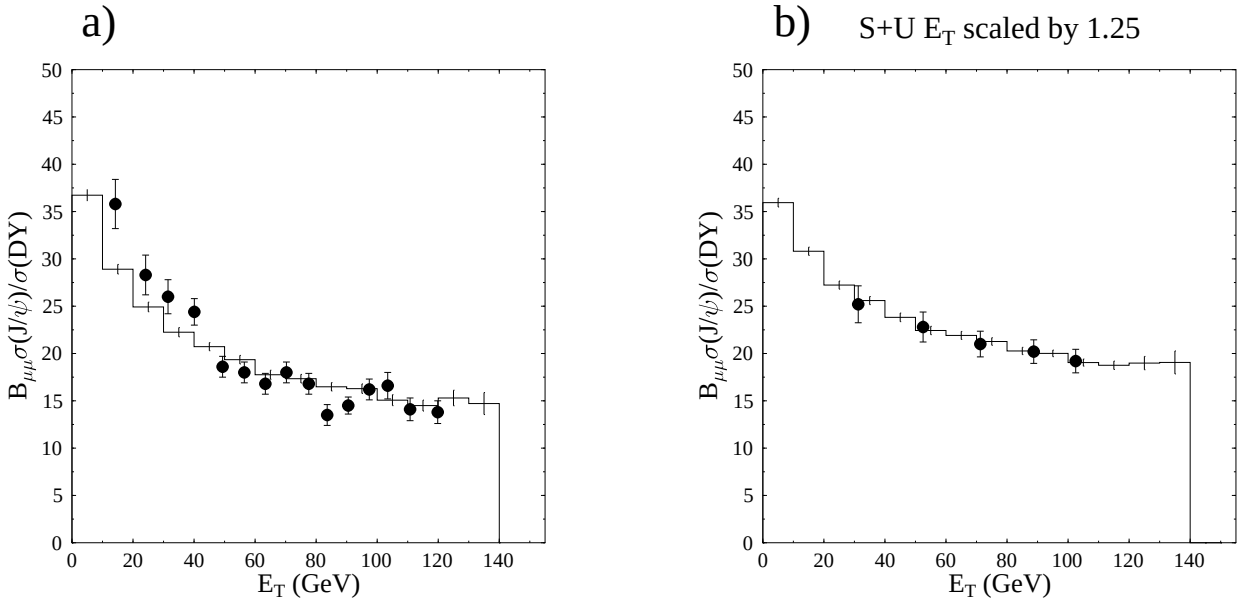

FIG. 9. The ratio of J/ψ to Drell-Yan production as a function of E_T for Pb+Pb collisions at 158 GeV (a) and S+U at 200 GeV (b) according to Scenario III. The experimental data are from Ref. [4] and [2], respectively. The normalization factor $B\sigma_\psi/\sigma_{\mu\mu} = 46$ in pp interactions at 200 GeV is taken from Ref. [11]. An additional factor of 1.25 [15] has been applied to the Pb+Pb calculation in order to account for the lower energy (the J/ψ and the Drell-Yan cross section have a different energy dependence). The E_T values of the experimental S+U data from [2] are scaled by a factor 1.25 assuming that the UrQMD calculation reflects the correct E_T distribution, see Fig. 2.

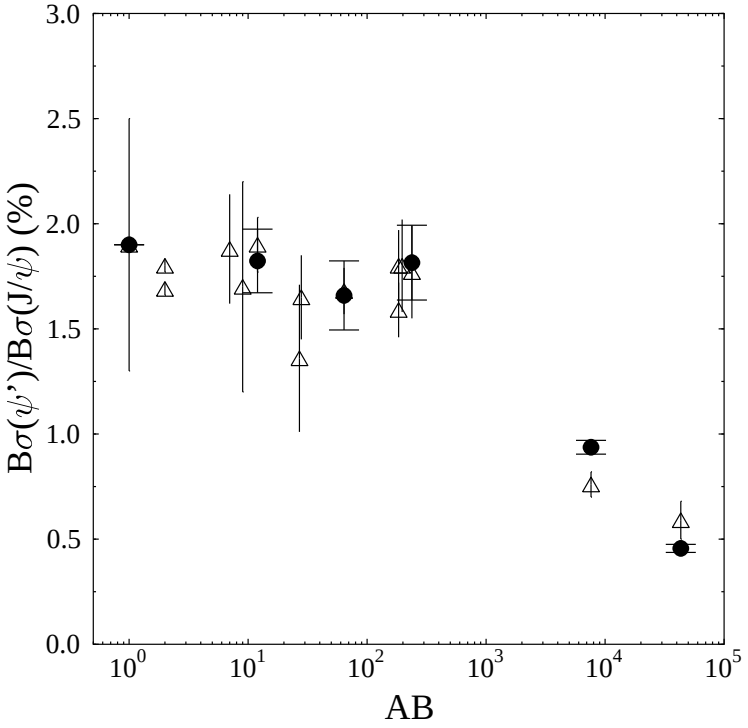

FIG. 10. $\psi'/J/\psi$ ratio in pA, S+U and Pb+Pb interactions as function of AB for universal nuclear dissociation cross sections and distinct charmonium states interacting with comovers after their formation time, Scenario II. The data (open triangles) are from [2,56].

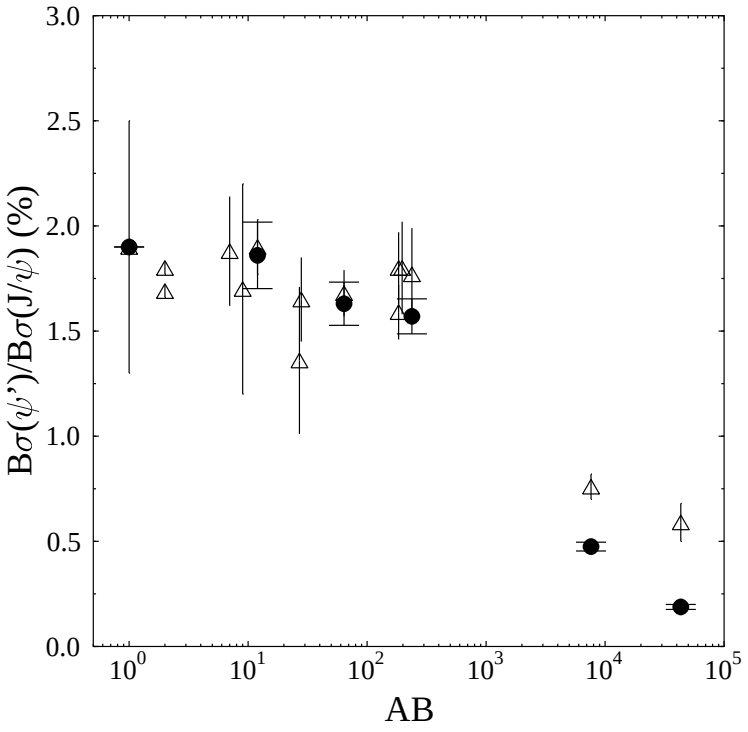

FIG. 11. $\psi'/J/\psi$ ratio in pA, S+U and Pb+Pb interactions as function of AB for evolving dissociation cross sections, Scenario III. The data (open triangles) are from [2,56].

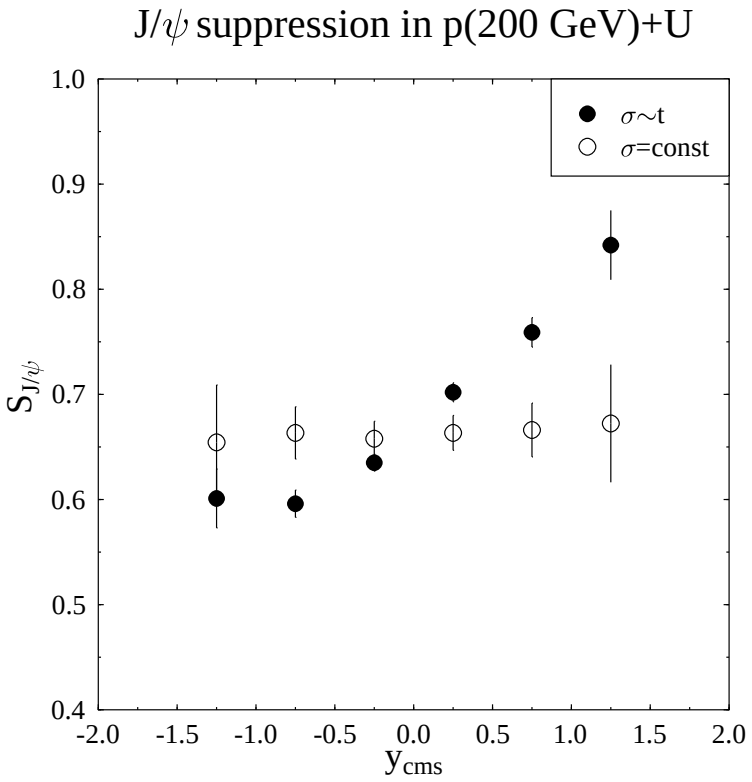

FIG. 12. J/ψ-survival probability in p(200 GeV)+U reactions as a function of rapidity. Calculations with Scenario II (open circles) and Scenario III (full circles) are shown.

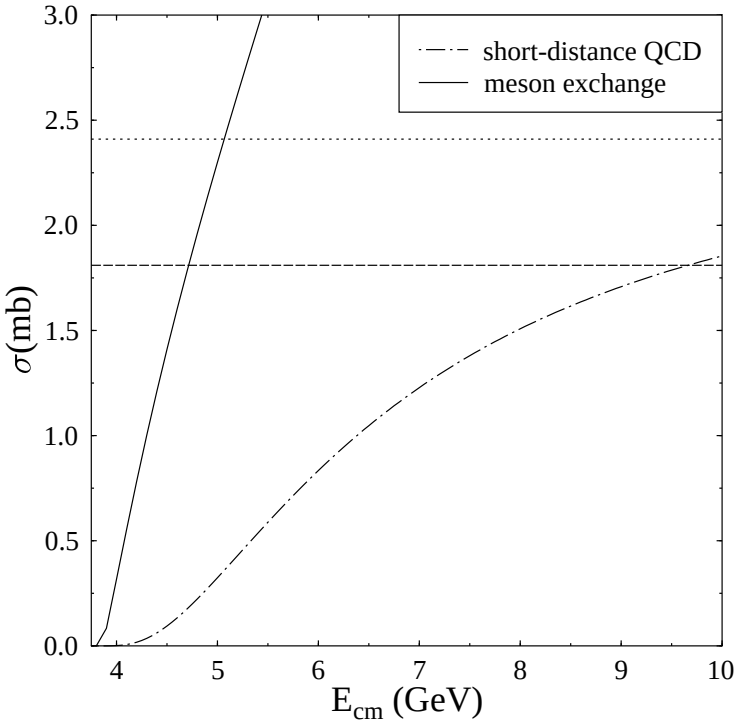

FIG. 13. $J/\psi\,\pi$ dissociation cross section as calculated in short-distance QCD according to [34] in comparison with a calculation with a meson exchange model [24]. Also shown are the values of the J/ψ-meson absorption cross section chosen for the model calculations with evolving cross sections, $\sigma = 2.4$ mb (Scenario III), and for the calculations with constant cross sections, color-octet nuclear absorption and no leading mesons, $\sigma = 1.8$ mb (Scenario II).

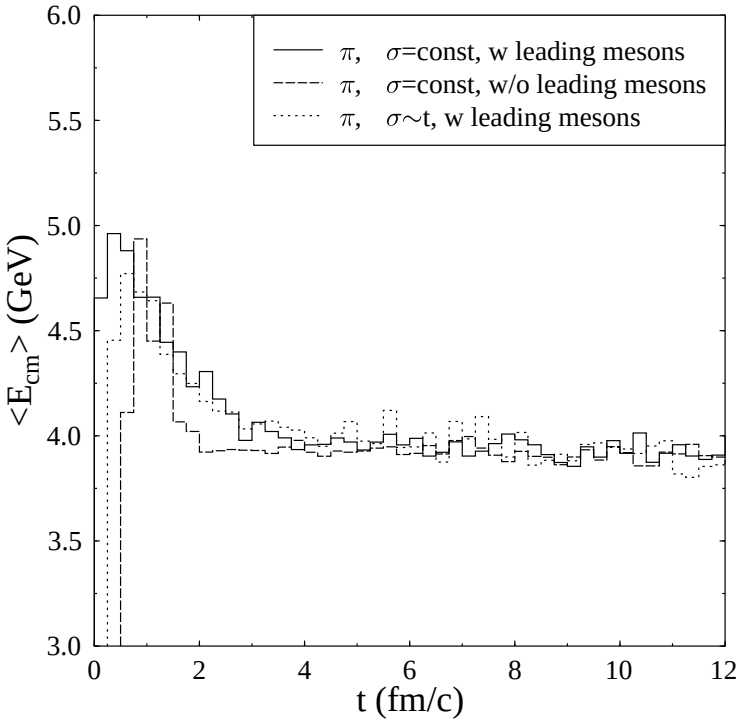

FIG. 14. Average $J/\psi\,\pi$ collision energies in central Pb(160 GeV)+Pb reactions as a function of time for different comover scenarios. We show the distributions for constant dissociation cross sections including leading meson interactions (full line), excluding leading mesons, Scenario II (dashed line) and for evolving cross sections with leading mesons, Scenario III (dotted line).

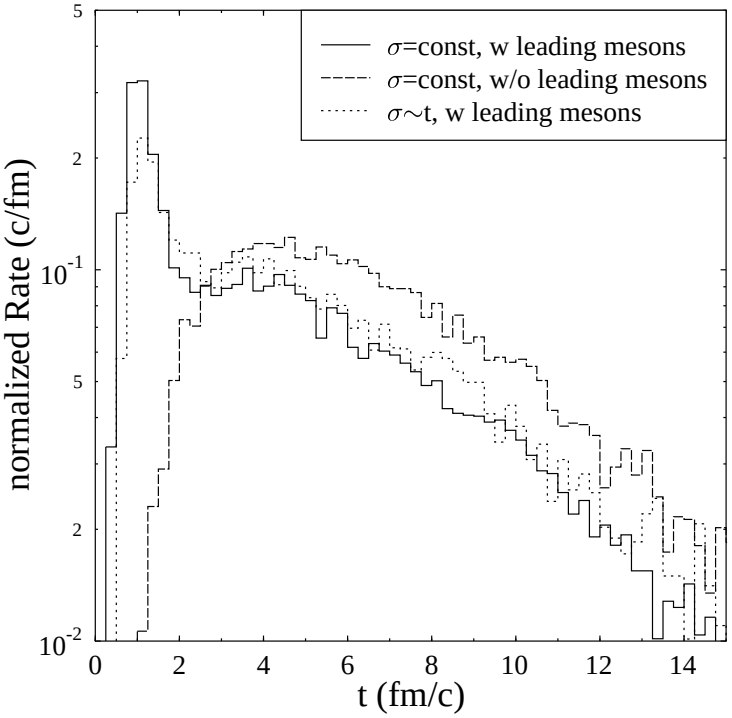

FIG. 15. J/ψ-meson collision rates, normalized to one dissociation, in central Pb(160 GeV)+Pb reactions as a function of time. We show the results for constant dissociation cross sections including leading meson interactions (full line), excluding leading mesons, Scenario II (dashed line) and for evolving cross sections with leading mesons, Scenario III (dotted line).

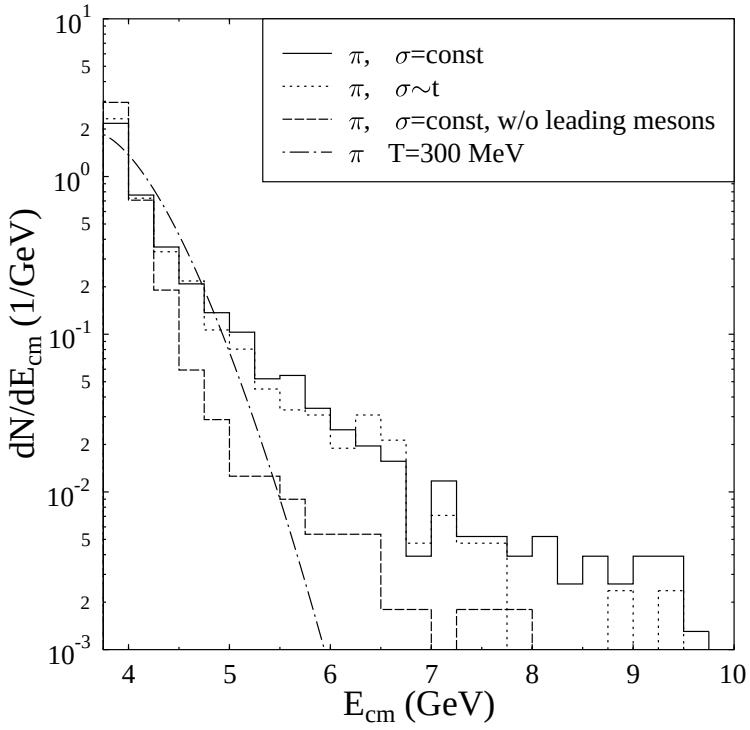

FIG. 16. Time integrated $J/\psi\,\pi$ collision spectrum in central Pb(160 GeV)+Pb reactions according to the UrQMD calculation (normalized to one collision) in comparison to a thermal hadron gas. Shown are the energy spectra resulting from constant dissociation cross sections including leading meson interactions (full line), excluding leading mesons, Scenario II (dashed line) and for evolving cross sections with leading mesons, Scenario III (dotted line). The $J/\psi\,\pi$ collision spectrum in an ideal gas of π's at $T = 300$ MeV is indicated by the dash-dotted curve.

REFERENCES

[1] C. Baglin *et al.* (NA38 Collab.), Phys. Lett. **B251** (1990) 472; Phys. Lett. **B270** (1991) 105; Phys. Lett. **B345** (1995) 617.
[2] M. Gonin *et al.* (NA50 Collab.), Nucl. Phys. **A610** (1996) 404c.
[3] M.C. Abreu *et al.* (NA50 Collab.), Phys. Lett. **B410** (1997) 327, 337.
[4] A. Romana (NA50 Collab.), in Proceedings of the XXXIIIrd Rencontres de Moriond, March 1998, Les Arcs, France.
[5] C. Gerschel and J. Hüfner, Phys. Lett. **B207** (1988) 253.
[6] C. Gerschel and J. Hüfner, Z. Phys. **C56** (1992) 171.
[7] S. Gavin, H. Satz, R.L. Thews and R. Vogt, Z. Phys. **C61** (1994) 351; S. Gavin, Nucl. Phys. **A566** (1994) 287c.
[8] J.-P. Blaizot and J.-Y. Ollitrault, Phys. Rev. Lett. **77** (1996) 1703.
[9] S. Gavin and R. Vogt, Phys. Rev. Lett. **78** (1997) 1006.
[10] C.-Y. Wong, Phys. Rev. **C55** (1997) 2621; Contribution to the *Workshop on Quarkonium Production in Relativistic Nuclear Collisions*, Seattle, May 1998, hep-ph/9809497.
[11] D. Kharzeev, C. Lourenco, M. Nardi and H. Satz, Z. Phys. **C74** (1997) 307.
[12] R. Vogt, Phys. Lett. **B430** (1998) 15.
[13] N. Armesto and A. Capella, Phys. Lett. **B430** (1998) 23; N. Armesto, A. Capella and E.G. Ferreiro, hep-ph/9807258.
[14] T. Matsui and H. Satz, Phys. Lett. **B178** (1986) 416.
[15] R. Vogt, LBNL-41758, Phys. Rep., in press.
[16] D. Kharzeev, in Proceedings of Quark Matter '97, Tsukuba, Japan, Nucl. Phys. **A638** (1998) 279c.
[17] B. Müller, DUKE-TH-98-145, Talk given at the CERN Heavy Ion Forum, June 1997, nucl-th/9806023.
[18] S.A. Bass, M. Gyulassy, H. Stöcker and W. Greiner, hep-ph/9810281, J. Phys. **G**, in press.
[19] S. Gavin, M. Gyulassy and A. Jackson, Phys. Lett. **B207** (1988) 257.
[20] R. Vogt, M. Prakash, P. Koch and T.H. Hansson, Phys. Lett. **B207** (1988) 263.
[21] D. Neubauer, K. Sailer, B. Müller, H. Stöcker and W. Greiner, Mod. Phys. Lett. **A4** (1989) 1627.
[22] K. Martins, D. Blaschke and E. Quack, Phys. Rev. **C51** (1995) 2723.
[23] L. Gerland, L. Frankfurt, M. Strikman, H. Stöcker and W. Greiner, Phys. Rev. Lett. **81** (1998) 762.
[24] S.G. Matinian and B. Müller, Phys. Rev. **C58** (1998) 2994.
[25] W. Cassing and C. M. Ko, Phys. Lett. **B396** (1997) 39.
[26] W. Cassing and E.L. Bratkovskaya, Nucl. Phys. **A623** (1997) 570.
[27] H. Sorge, E. Shuryak and I. Zahed, Phys. Rev. Lett. **79** (1997) 2775.
[28] J. Geiss, C. Greiner, E.L. Bratkovskaya, W. Cassing and U. Mosel, nucl-th/9803008.
[29] D.E. Kahana and S.H. Kahana, nucl-th/9808025.
[30] C. Spieles, R. Vogt, L. Gerland, S.A. Bass, M. Bleicher, L. Frankfurt, M. Strikman, H. Stöcker, W. Greiner, LBNL-42410, hep-ph/9810486.
[31] D.M. Alde *et al.* (E772 Coll.), Phys. Rev. Lett. **64** (1990) 2479.
[32] C. Baglin *et al.* (NA38 Collab.), Phys. Lett. **B262** (1991) 362.
[33] G.A. Alves *et al.* (E769 Collab.), Phys. Rev. Lett. **70** (1993) 722.

[34] D. Kharzeev and H. Satz, Phys. Lett. **B334** (1994) 155.
[35] J. Badier *et al.* (NA3 Coll.), Z. Phys. **C20** (1983) 101.
[36] D.M. Alde *et al.* (E772 Coll.), Phys. Rev. Lett. **66** (1991) 133.
[37] D.S. Barton *et al.*, Phys. Rev. **D27** (1983) 2580.
[38] S.A. Bass *et al.*, Prog. Part. Nucl. Phys. **41** (1998) 225; version 1.1 of the code is publicly available from http://www.th.physik.uni-frankfurt.de/~urqmd/urqmd.html.
[39] J. Konopka, PhD thesis, J. W. Goethe University, Frankfurt am Main (1996); S.A. Bass, PhD thesis, J. W. Goethe University, Frankfurt am Main (1997).
[40] R. Gavai, D. Kharzeev, H. Satz, G.A. Schuler, K. Sridhar and R. Vogt, Int. J. Mod. Phys. **A10** (1995) 3043.
[41] R. Vogt, Atomic Data and Nuclear Data Tables **50** (1992) 343.
[42] T. Alber *et al.*, Phys. Rev. Lett. **75** (1995) 3814.
[43] L. Ramello (NA50 Collab.), in Proceedings of Quark Matter '97, Tsukuba, Japan, Nucl. Phys. **A638** (1998) 261c.
[44] A. Borhani (NA38 Collab.), Ph.D. thesis, Ecole Polytechnique, Palaiseau (1996).
[45] G.A. Schuler, CERN Preprint, CERN-TH-7170-94, hep-ph/9403387.
[46] L. Kluberg (NA50 Collab.), Proceedings of the Conference on *Heavy Ion Collisions from Nuclear to Quark Matter*, September 1998, Erice, Italy.
[47] D. Kharzeev, M. Nardi and H. Satz, hep-ph/9707308.
[48] M. Nardi and H. Satz, hep-ph/9805247.
[49] NA49 Collab. (H. Appelshäuser *et al.*), Eur. Phys. J. **C2** (1998) 661.
[50] M. Bleicher, C. Spieles, C. Ernst, L. Gerland, S. Soff, H. Stöcker, W. Greiner and S.A. Bass, hep-ph/9803346, Phys. Lett. **B** in press.
[51] NA35 Collab. (J. Bächler *et al.*), Phys. Rev. Lett. **72** (1994) 1419.
[52] NA49 Collab. (H. Appelshäuser *et al.*), nucl-ex/9810014v2.
[53] WA98 Collab. (M.M. Aggarwal *et al.*), Phys. Rev. Lett **81** (1998) 4087.
[54] G. Roland (NA49 Collab.), Proceedings of Hirschegg '97: QCD Phase Transitions, p. 309, GSI, Darmstadt. M. Bleicher, M. Belkacem, C. Ernst, H. Weber, L. Gerland, C. Spieles, S.A. Bass, H. Stöcker, W. Greiner, Phys. Lett. **B435** (1998) 9.
[55] T. Alber *et al.* (NA35 Coll.), Eur. Phys. J. **C2** (1998) 643.
[56] C. Lourenco, Nucl. Phys. **A610** (1996) 552c.
[57] L. Frankfurt and M. Strikman, Prog. Part. Nucl. Phys. **27** (1991) 135,
J. Hüfner and B.Z. Kopeliovich, Phys. Rev. Lett. **76** (1996) 192.
[58] J.-W. Chen and M. Savage, Phys. Rev. **D57** (1998) 2837.
[59] R. Vogt, in preparation.
[60] C. Spieles, R. Vogt, L. Gerland, S.A. Bass, M. Bleicher, H. Stöcker and W. Greiner, LBNL-42280, hep-ph/9809441.